A General Framework for Convective Trigger Functions

ROBERT F. ROGERS AND J. M. FRITSCH

Department of Meteorology, The Pennsylvania State University, University Park, Pennsylvania

(Manuscript received 15 December 1995, in final form 25 April 1996)

ABSTRACT

A general framework for the trigger function used in convective parameterization routines in mesoscale models is proposed. The framework is based on the diagnosis of the accessibility of potential buoyant energy. Specifically, the trigger function 1) estimates the magnitude of the largest vertical velocity perturbation from a source layer and 2) calculates the total amount of inhibition between the source layer and the level of free convection. The calculation of perturbation magnitude accounts for such factors as subgrid-scale inhomogeneities, a convective boundary layer, and convergence within the source layer. Specific formulations to quantify these factors are proposed.

The trigger is tested in a simulation using the PSU–NCAR mesoscale model MM5. The event chosen for simulation is a summertime case exhibiting a variety of environments. The results of this simulation are compared with a simulation using the Fritsch–Chappell (FC) trigger function. It is found that decisions made by the new trigger function are more physically consistent with the local environment than decisions made by the FC trigger.

1. Introduction

The problem of convective parameterization is widely recognized by the modeling community to be a crucial component in obtaining successful numerical simulations and forecasts (Emanuel and Raymond 1993). Consequently, much energy has been exerted in developing parameterizations that realistically reflect the effects of convection on resolvable-scale fields. However, comparatively little attention has been given to developing criteria for determining when and where deep convection will occur. Such criteria are collectively termed the convective "trigger function." It has been shown (e.g., Kain and Fritsch 1992; Stensrud and Fritsch 1994) that some simulations are highly sensitive to what sort of trigger function is used. When and where convection occurs in a given model simulation influences the vertical distribution of heating, the propagation of gravity waves from the convection, the movement of outflow boundaries, and many other nonlinear feedbacks that can substantially alter the results of the simulation. Thus it is crucial to develop a trigger function that can accurately diagnose the timing and location of convection.

Recent advances in both our understanding of the atmosphere and in computing power have allowed operational and research numerical models to have much finer resolutions (e.g., $\Delta X \sim 15$–30 km) than were previously possible. Consequently, these models are now capable of resolving many of the mesoscale features that contribute significantly to determining the timing and location of convection. Conceptually, then, it should be possible to improve the diagnosis of the onset of convection in mesoscale models. However, because many of the current parameterization schemes were designed for synoptic- and/or global-scale models, the dynamical constraints that the current schemes use to relate convection to grid-resolvable circulations may be different from those that are valid for mesoscale models. Thus, it is questionable whether or not the criteria used to place convection in larger-scale models, such as moisture or mass convergence (Kuo 1974) or grid-scale destabilization rate (Arakawa and Schubert 1974), can be applied successfully to finer-resolution mesoscale models.

In view of the above considerations, many of the parameterization schemes designed for mesoscale models—such as Kreitzberg and Perkey (1976), Fritsch and Chappell (1980), Frank and Cohen (1985), and Kain and Fritsch (1993)—use alternate methods to diagnose the onset of convection. These schemes rely on the concept of the accessibility of potential buoyant energy to trigger convection. For example, the Fritsch–Chappell (FC) and Kain–Fritsch (KF) schemes compute the amount of inhibition that a parcel must overcome while rising from its lifting condensation level (LCL) to its level of free convection (LFC). This is done by integrating the parcel buoyancy equation over that layer and is analogous to determining the amount of negative area between the LCL and the LFC on a skew T diagram. In an attempt to repre-

Corresponding author address: Robert F. Rogers, Department of Meteorology, The Pennsylvania State University, 503 Walker Building, University Park, PA 16802-5013.

sent the fact that surface-based hygrothermal and/or vertical velocity perturbations can be modified by mesoscale air motions (Chen and Orville 1980), the ability of the parcel to overcome the inhibition is modified by the resolvable-scale vertical velocity at the LCL. Weaknesses in this formulation lie in both the specification of perturbation magnitudes based on mesoscale forcing (a firm quantitative link between the two has not yet been established) and in the computation of the amount of inhibition that must be overcome before convection can be initiated. In FC and KF, the only negative area that is considered is that between the LCL and the LFC. Inhibition that a parcel encounters between the layer from which it originated (its source layer) and the LCL is not accounted for, even though in many cases there can be an appreciable amount of negative area within this layer.

The purpose of this study is to identify and explore the trigger function weaknesses for forecasting convection in mesoscale models and to propose a new trigger function that provides a framework for correcting some of the weaknesses. This new trigger function is tested in a mesoscale model and compared with the same simulation using the original version of the Fritsch–Chappell trigger function (Fritsch and Chappell 1980). The comparison is used to highlight the validity of the assumptions underlying both triggers and to encourage consideration of the important issue of how to initiate convection in mesoscale models. Section 2 defines the new trigger function formulation, and section 3 describes the mesoscale model and the case used in the testing. The results of the comparisons are presented in section 4. Section 5 provides a summary and concluding remarks.

2. Description of the trigger

An important and desirable property of a trigger function formulation is applicability to a wide variety of environments, ranging from well-mixed, free convective boundary layers to stably stratified, nocturnal boundary layers. In order to construct a function with such wide applicability, the following two steps are adopted as the general basis for the triggering decision:

1) estimation of the magnitude of the largest subgrid-scale vertical velocity perturbation originating from within each potential source layer, and
2) calculation of whether or not this perturbation is strong enough to overcome the total grid-resolvable negative inhibition between the source layer and the LFC.

Factors that influence the determination of perturbation magnitudes are discussed in the next subsection, and the formulation and implementation of the trigger are discussed in the following subsection.

a. Vertical velocity perturbations

The magnitude of the vertical velocity perturbations is influenced by many factors such as insolation and local inhomogeneities in surface physiography and/or atmospheric structure. Over the past decade, surface heterogeneity (e.g., rough or steep terrain, land/water interfaces, and vegetative coverage differences) has received much attention (e.g., Avissar and Pielke 1989; Chen and Avissar 1994; Hong et al. 1995) because of the role it plays in triggering convection, especially during the warm-season daytime hours. These surface variations, as well as other features such as cloud-scale outflow boundaries, are often unresolved in mesoscale models with resolutions on the order of 10 km or greater. Parameterizing the effect of subgrid-scale inhomogeneities on vertical velocity perturbations is therefore necessary.

Although there is likely a spectrum of perturbation sizes in a given grid element, intuitively, the largest (in areal coverage) and most buoyant perturbations are the ones that have the greatest probability of reaching the LFC and triggering convection. For grid elements with more and/or stronger inhomogeneities, there is likely a greater number of relatively stronger perturbations. Thus, formulations for estimating perturbation magnitudes in a given grid cell should be directly dependent on the degree of inhomogeneity in the cell.

Since no database exists that contains all measures of inhomogeneity for every grid point in a model, it is necessary to estimate the spectrum of subgrid-scale perturbations by other means. One approach is to assign a grid-size dependence to the inhomogeneity spectrum. This approach stems from the recognition that there should be more and larger subgrid-scale features that create inhomogeneities within larger grid elements; that is, other things being equal, for a larger grid size, it is more likely that there will be more and larger perturbations. Thus, given the same amount of convective inhibition, convection is more likely to occur in large grid elements than in small ones. Also, because many of the perturbations arise from inhomogeneities that exist at the surface, the perturbation should be dependent upon the properties of the surface (e.g., variations in terrain, vegetation, soil moisture, etc.), the height above the surface (Segal et al. 1989), and the stability between the surface and the layer from which the rising parcel emanates (i.e., the source layer).

Another important factor that affects the magnitude of subgrid-scale perturbations is the strength of the diurnal heating cycle. In cases of strong daytime heating, free convective boundary layers, which often serve to trigger convection, can develop. Subgrid-scale perturbations originating in such layers have a vertical velocity that can be described by the free convective scaling velocity w^*, which is a function of the surface buoyancy flux and the height of the top of the planetary boundary layer (Stull 1988). The value of w^* can be

obtained from a high-resolution boundary layer model (Zhang and Anthes 1982).

If the source layer is above a free convective boundary layer, the effect of the surface-driven thermals may still trigger convection. When the thermals reach the top of the boundary layer, they typically encounter negative area (unless, of course, they have reached their level of free convection). As the thermals overshoot and penetrate into the negative area, they are forcing air above them upward because of their own upward motion. This upward motion serves as a vertical velocity perturbation for layers above the free convective boundary layer (Clark et al. 1986). Based upon this work, the magnitude of these perturbations should increase as w^* increases and decay rapidly with increasing height and stability above the boundary layer top.

Of course, many cases of convection occur when boundary layer air is convectively stable. In these cases, convection originates from a source above the stable boundary layer and in an area in which the environment is nearly saturated. This situation typically occurs as moist low-level air overruns a warm front or a convective outflow boundary. In these regimes, vertical velocity perturbations resulting from surface-based inhomogeneities may be very small or nonexistent. Perturbations can still arise, however, from free-atmosphere processes such as Kelvin–Helmholtz waves or gravity waves.

Yet another factor that appears to influence the magnitude of subgrid-scale perturbations is convergence in the source layer. Based upon Chen and Orville (1980), convergence serves to organize and strengthen perturbations such that they are more likely to reach their level of free convection. Conversely, divergence tends to weaken and suppress perturbations. Thus, the magnitudes of existing vertical velocity perturbations in a given layer should be modified commensurate with the amount of convergence or divergence in that layer.

b. *Formulation and implementation of trigger*

In order to test the concepts presented above, specific relationships that quantify the effects of inhomogeneities, surface heating, convergence, etc. on the magnitude of subgrid-scale vertical velocity perturbations must be defined. Unfortunately, neither theoretical nor empirical formulations for the exact functional dependencies of these parameters on resolvable scales are available. Therefore, rudimentary relationships describing these functionalities are prescribed below as a framework within which to test the concepts.

As a starting point, it is assumed that the magnitude of the largest vertical velocity perturbation w_p, not accounting for grid-scale convergence, can be expressed as the sum of the contributions from inhomogeneities and from the convective boundary layer, if such a boundary layer exists. The vertical velocity perturbation arising from inhomogeneities is specified by

$$w_i = k_1 \frac{\Delta x}{L}\left(1 - \frac{h_{SL}}{H}\right), \qquad (2.1)$$

where k_1 is a coefficient of proportionality that varies in space as a function of surface properties (without any data upon which to determine such a functionality, k_1 is assumed here to be constant at 0.2 m s^{-1}), Δx is the grid size (m), L is the grid-length scale beneath which cloud-scale perturbations begin to become resolved explicitly, h_{SL} is the midheight of the source layer above the ground in meters, and H is the threshold height above which surface-based and lower-tropospheric perturbations are assumed to become negligible. In the preliminary tests presented in section 4, L = 10 km and H = 5 km. Based upon this formulation, the value of w_i increases with increasing grid size (Δx) and decreases with increasing height above the surface (h_{SL}).

The convective boundary layer perturbation (w_{cbl}) is set equal to w^* for cases where the source layer is within a convective boundary layer. The determination of a convective boundary layer is made by the boundary layer scheme employed by the mesoscale model (Zhang and Anthes 1982). For source layers above the convective boundary layer, the following relationship is assumed:

$$w_{abl} = w_{cbl} \exp - \left[c_1 (\Delta z_A)^2 + \frac{c_2}{\bar{\theta}_v} \frac{\partial \theta_v}{\partial z} \right], \qquad (2.2)$$

where Δz_A (m) is the distance between the top of the boundary layer and the midheight of the source layer (h_{SL}), $\bar{\theta}_v$ is the mean virtual potential temperature (K) between the boundary layer top and the source layer, $\partial\theta_v/\partial z$ is the stability within the layer Δz_A, and c_1 and c_2 are proportionality constants set to 5×10^{-7} m^{-2} and 3×10^4 m, respectively. These values of c_1 and c_2 have been specified such that the two terms in parentheses have approximately the same order of magnitude, and hence both affect w_{abl}, given typical values of Δz_A, $\bar{\theta}_v$, and $\partial\theta_v/\partial z$. This formulation allows for exponential decay of w_{abl} as a function of height and stability above the boundary layer. It is an attempt to quantify relationships that were found in Clark et al. (1986). In their modeling study they found that, for a given value of stability, the magnitudes of the vertical velocity perturbations decreased between 50% and 80% over a 2-km depth above the convective boundary layer. Figure 1 shows w_{abl} as a function of depth (Δz_A) between the boundary layer top and the source layer midheight for assumed values of w_{cbl} = 1.0 m s^{-1}, $\bar{\theta}_v$ = 300 K, and $\partial\theta_v/\partial z$ = 1 K km^{-1} and also as a function of stability ($\partial\theta_v/\partial z$) for Δz_A = 500 m and $\bar{\theta}_v$ = 300 K. For this formulation, the magnitude of the vertical velocity perturbation decreases 80% at a depth of 2 km above the boundary layer. The decrease in magnitude of the vertical velocity perturbation is not as sensitive to changes

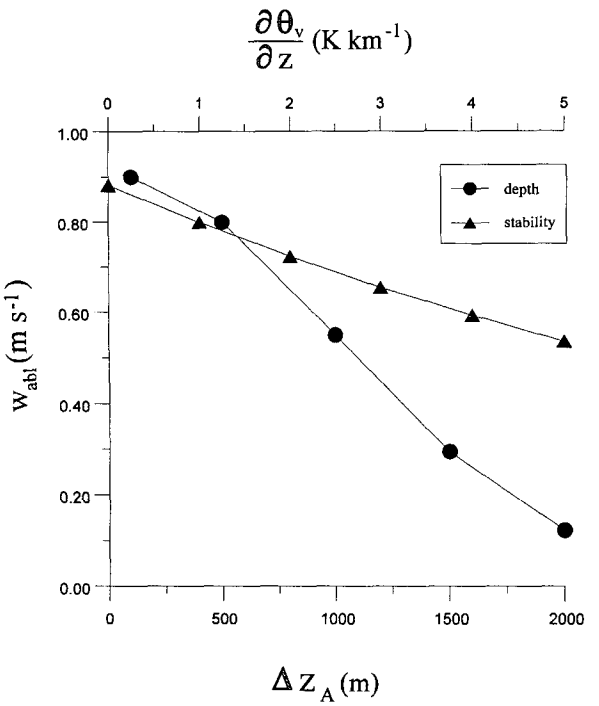

FIG. 1. Plot of w_{abl} as a function of Δz_A for assumed values of w_{cbl} = 1.0 m s^{-1}, $\bar{\theta}_v$ = 300 K, and $\partial\theta_v/\partial z$ = 1 K km^{-1}, and as a function of $\partial\theta_v/\partial z$ for assumed values of w_{cbl} = 1.0 m s^{-1}, Δz_A = 500 m, and $\bar{\theta}_v$ = 300 K.

in stability, however, decreasing only 30% as the stability increases to 5 K km^{-1}.

The total of the contributions from inhomogeneities and from the convective boundary layer can now be expressed as

$$w_p = w_i + w_{cbl} + w_{abl}, \tag{2.3}$$

where w_{abl} is zero if the source layer is within a convective boundary layer, w_{cbl} is zero if the source layer is above a convective boundary layer, and both are zero if no convective boundary layer exists. Since subgrid-scale inhomogeneities create perturbations regardless of the type of boundary layer that exists, w_i is always computed. If the boundary layer is free convective, then w_{cbl} or w_{abl} is computed, depending on whether the source layer is within or above the boundary layer, respectively.

A final estimate of the magnitude w' of the largest vertical velocity perturbation is obtained by increasing (decreasing) w_p to account for convergence (divergence) in the source layer. Specifically, the magnitude of w_p is modified by the following formulation:

$$w' = w_p\left[1 + c_3\left(\frac{\partial \omega_{res}}{\partial p}\right)^{1/3}\right], \tag{2.4}$$

where $\partial\omega_{res}/\partial p$ is the vertical derivative in pressure coordinates of the resolvable-scale vertical motion (equal to the divergence in the layer being considered) and c_3 is a proportionality constant set to 10 s$^{1/3}$. This value of c_3 was chosen to provide magnitudes of w' that fall within the range of observed values of eddy vertical motions (see Khalsa and Greenhut 1985). For example, when convergence is 10^{-5} s^{-1}, w_p is increased by about 20%. When convergence is 10^{-4} s^{-1}, w_p is increased by about 50%. Equation (2.4) is applied only in the source layer.

Beginning with the model layer closest to the ground, the thermodynamic properties of adjacent layers overhead are mixed in a mass-weighted fashion until the combined depth of the mixture (the source layer) is a least 60 mb (the actual depth may vary slightly due to differences in the thicknesses of the individual model layers). The perturbation vertical velocity is then determined for that particular source layer. The next step is to compute the inhibition energy (E_i, commonly known as the negative area) for the layer between h_{SL} and the LFC. This is accomplished by integrating the parcel buoyancy equation, that is,

$$E_i = w_{neg}^2 = 2g\frac{\theta_{ve} - \theta_v'}{\theta_{ve}}\Delta z_{LFC}, \tag{2.5}$$

where w_{neg} is the vertical velocity that a perturbation would need to overcome the inhibition energy, g is the acceleration due to gravity, θ_{ve} is the virtual potential temperature of the environment, θ_v is the virtual potential temperature of the parcel, and Δz_{LFC} is the layer between the source layer and the LFC being considered for the negative area computation. If the following condition exists,

$$w' \geq w_{neg}, \tag{2.6}$$

then the parcel can overcome the layer of inhibition and convection can occur. If not, then a 60-mb-deep layer beginning with the second-lowest model layer is checked in the same way, and so on, until a buoyant mixture is found or each layer in the lowest 300 mb has been tested and found to be nonbuoyant.

3. Experimental design

In order to test the trigger function presented above, a case that exhibited a variety of convective environments was selected for simulation using the Pennsylvania State University–National Center for Atmospheric Research Mesoscale Model Version 5 (PSU–NCAR MM5) (Grell et al. 1994). The case chosen for simulation occurred on 14 July 1982 and involved the development of a series of mesoscale convective systems (MCSs) over the western Plains states and the Front Range of the Rocky Mountains. In particular, during the afternoon and evening of 14 July 1982, six distinct MCSs formed in a line stretching from Saskatchewan southward to New Mexico. For this study two simulations are performed: one using the new trig-

ger function, and one using the Fritsch–Chappell trigger function. The model is statically initialized at 1200 UTC 14 July 1982 and is run for 12 h in each simulation.

To perform the comparisons between the two trigger functions, the evolution of the model-simulated convection using each trigger function is compared with the observed convection. More importantly, since the model-simulated evolution of convection may be in error for many reasons that have little to do with the trigger function (e.g., errors in the initial conditions, inadequate boundary layer parameterization, etc.), soundings at three grid points representing a variety of environments are examined closely in an attempt to determine how well each trigger function diagnoses the decision of convective initiation based on the model-generated soundings. Given the wide spectrum of synoptic environments that occur in this particular case, it is a severe test of the trigger functions' ability to discern the likelihood for convective activity. In the following sections, brief descriptions of the mesoscale model and the synoptic conditions during the event are presented.

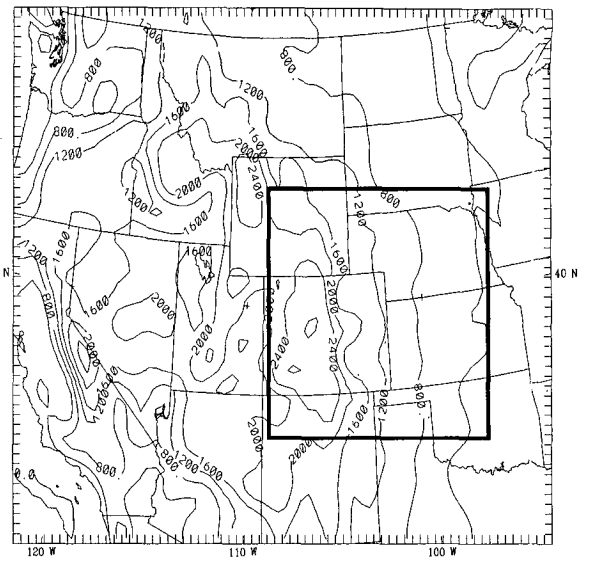

FIG. 2. Coarse- and fine-mesh domains. Bold lines indicate position of fine-mesh domain. Thin lines indicate coarse-mesh terrain. Contour interval is 400 m.

a. Description of the model

The PSU–NCAR MM5 is a primitive equation, nonhydrostatic, three-dimensional model. The domain configuration consists of a two-way interactive nested grid (Zhang et al. 1986) with a coarse-mesh resolution of 36 km and a fine-mesh resolution of 12 km. The locations of the two domains, along with the coarse-mesh terrain, are shown in Fig. 2. The number of grid points for the (x, y, σ) dimensions of the coarse and fine meshes are (71, 55, 29) and (76, 88, 29), respectively. The spacing between sigma levels is smallest in the lower troposphere and increases with increasing height. Resolution is therefore concentrated in the lower troposphere in order to enhance the resolution of boundary layer processes (Stensrud 1992).

Numerous physical processes are represented in the model. In particular, resolvable-scale precipitation processes are simulated using an explicit moisture scheme that includes predictive equations for cloud water, cloud ice, rain, and snow (Dudhia 1989). This scheme is activated when grid-scale saturation is reached. For conditions at or below 0°C, the scheme allows for ice phase processes in which cloud water is treated as cloud ice and the remaining condensate is treated as snow. A high-resolution planetary boundary layer parameterization (Zhang and Anthes 1982) is used to simulate the vertical mixing of temperature, water vapor, momentum, and cloud water. The parameterization uses a surface energy budget that is dependent on the surface sensible and latent heat fluxes and the radiative fluxes. The radiative fluxes are calculated to account for the effects of clouds on both short- and longwave radiation. The scheme includes four different boundary layer regimes, ranging from stable to mechanically driven turbulence to forced convection to free convection.

To represent deep, moist convection in the model, the Kain and Fritsch (1993) parameterization scheme is used on both meshes. This scheme, like other parameterization schemes used in mesoscale models, estimates the subgrid-scale effects that convection has on such parameters as the vertical mass flux and the vertical profiles of temperature, moisture, and momentum. Two major questions are addressed by this scheme. First, it must determine whether or not convection will occur at a given grid point at a given time. This is accomplished by the trigger function. Second, if convection does occur at a grid point, the subgrid-scale effects of that convection on the resolvable scale must be calculated. This is accomplished by the cloud model. The cloud model in the Kain–Fritsch scheme includes both environmental entrainment and updraft detrainment. This entrainment–detrainment scheme allows the parameterized vertical distribution of convective heating and drying to be more responsive to environmental conditions than is possible with a traditional entraining plume model, such as that used in the Fritsch–Chappell scheme (Kain and Fritsch 1990). For this study, only the trigger function is varied between the two simulations. The cloud model is identical in both runs.

b. Synoptic conditions

At the model initialization time (1200 UTC 14 July 1982), the upper-air circulation over the western United States was dominated by a synoptic-scale disturbance centered over British Columbia and a negatively tilted ridge over the northern High Plains (Fig.

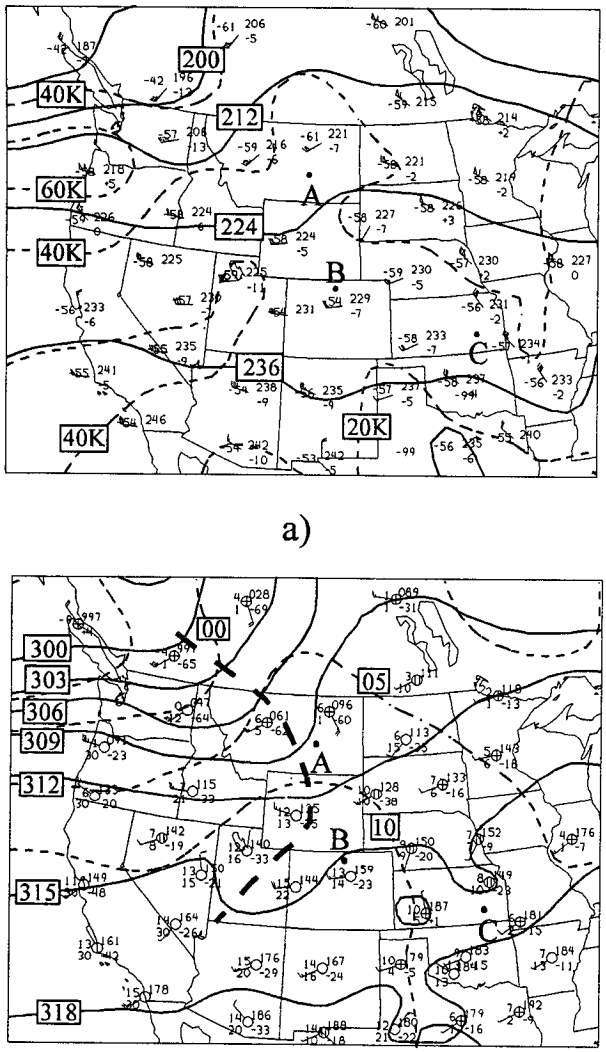

FIG. 3. Upper-air analyses at 1200 UTC 14 July for (a) 200 mb and (b) 700 mb. (a) Solid lines denote geopotential height (120-m contour interval), bold-dashed lines denote isotherms (5°C contour interval), and light-dashed lines denote isotachs (20-kt contour interval). Areas marked A, B, and C denote locations of the three grid points selected for detailed examination of trigger function performance. (b) Solid lines denote geopotential height (30-m contour interval), and dashed lines denote isotherms (5°C contour interval). Heavy-dashed line shows location of short-wave trough.

3). (The location of the three grid points selected for detailed examination of trigger function performance are indicated in Fig. 3.) Farther to the south, the upper-level flow was predominantly westerly, with a series of embedded weak short waves propagating eastward from the Pacific coast to the western Plains. Of particular note is the trough that extends from central Montana southwestward through central Utah. This trough passes over eastern Colorado during the next 12 h and influences the convective developments in the vicinity of grid points *B* and *C*.

At the surface, a weak frontal boundary stretched southeastward over the northern Great Plains, marking a shift from southerly to southeasterly flow (Fig. 4). This boundary formed an occlusion with a weak cold front over central Montana associated with the British Columbia disturbance. In advance of the short-wave trough over Colorado, a low-level southerly flow of moist air from the Gulf of Mexico covered much of the central and southern Plains (Fig. 4). Surface dewpoints of over 15°C covered a broad area extending northward from the gulf states to the prefrontal region in eastern Montana. In advance of this front, an area of deep convection had developed just north of grid point *A*, the first location that will be examined for trigger performance. Outflow from this convection coupled with the low-level southeasterly flow intercepting the front suggests that there was potential for additional deep convection in the vicinity of grid point *A*.

Although the surface data indicate only weak synoptic-scale features over the Great Plains, satellite imagery (Fig. 5) reveals at midmorning broken cloudiness over eastern Montana and Wyoming and western North and South Dakota, a decaying MCC over central Nebraska, broken cloudiness over western Oklahoma, and a developing area of convection over western Missouri. Otherwise, the rest of the Plains and Rocky Mountain states are under either thin cirrus clouds or clear skies. By midafternoon, eastern Montana was free of deep cloudiness, while cloudiness persisted over South Dakota and northern Nebraska in association with the frontal boundary located there. Also, areas of convection were continuing along the Kansas–Mis-

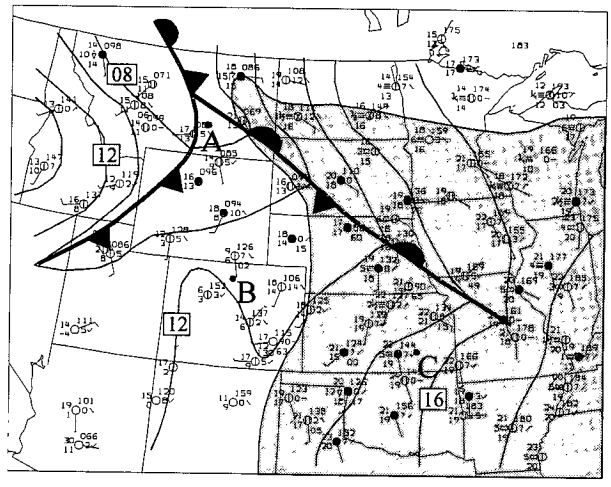

FIG. 4. Surface analysis for 1200 UTC 14 July 1982. The standard surface station data-plot convection is used. Solid lines are isobars (2-mb intervals). Shaded region shows areas where the dewpoint is greater than 15°C.

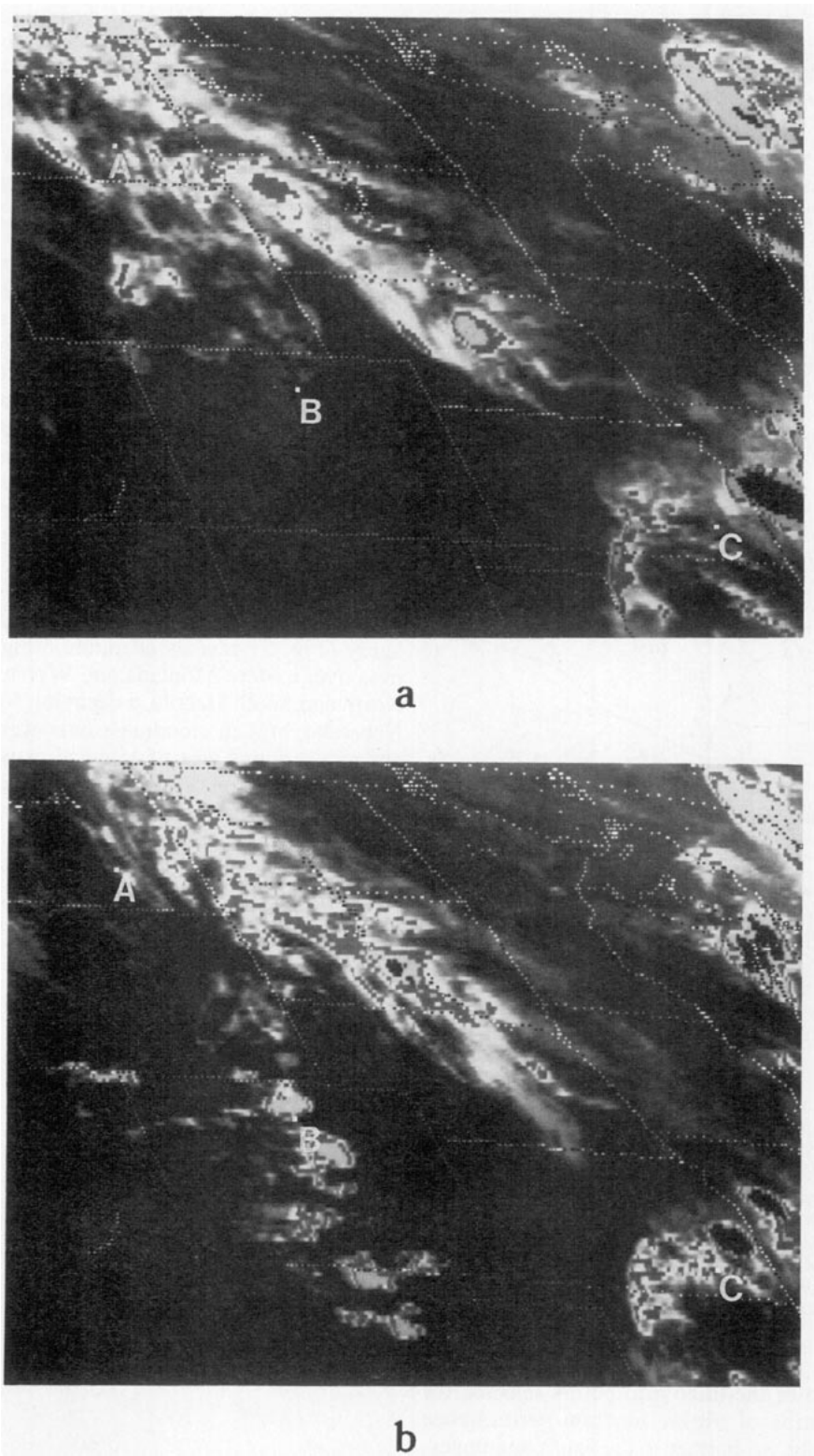

FIG. 5. Enhanced infrared satellite image for (a) 1515 UTC and (b) 1915 UTC 14 July 1982.

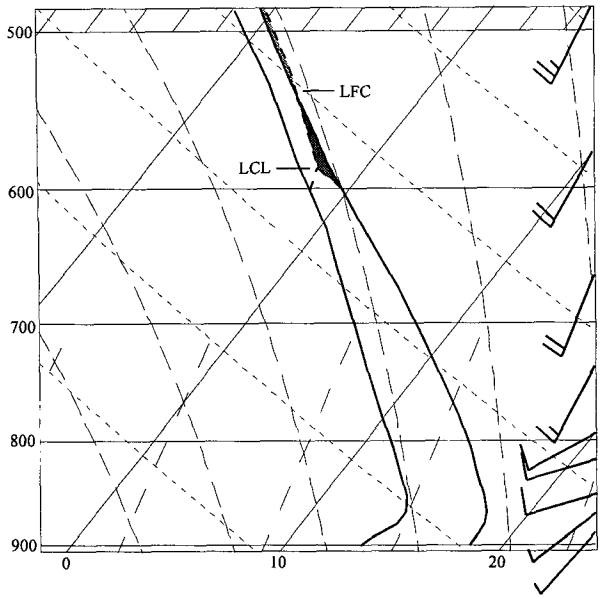

FIG. 6. Model-generated sounding for grid point *A* at 1200 UTC for the simulation using the FC trigger function. Bold-dashed line shows path followed by parcel originating from source layer determined by the trigger function (P_{SL} in subsequent tables). Dark-shaded region is convective inhibition encountered by parcel between its source layer and its LFC. Light-shaded region is convective available potential energy available to parcel undergoing undilute ascent.

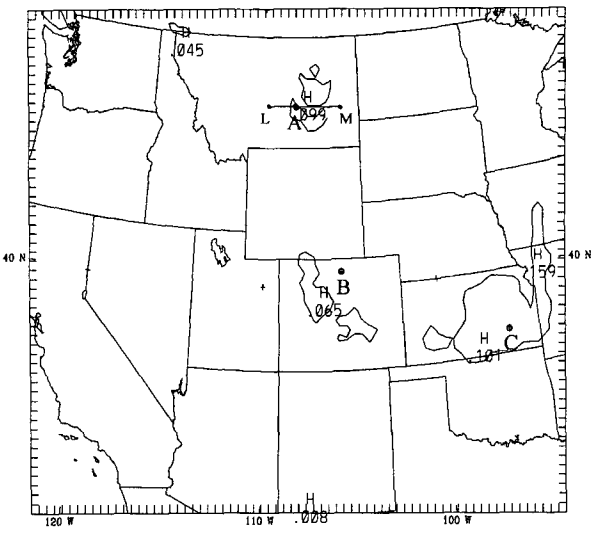

FIG. 7. One-hour accumulated convective rainfall for the coarse mesh ending at 1300 UTC using the FC trigger function. The value of the contour is 0.025 cm. Line *LM* shows location of cross sections in subsequent figures.

souri border and in a few areas along the Front Range of the Rocky Mountains in Colorado and New Mexico.

4. Trigger performances

As mentioned previously, three types of environments are selected for examining and comparing the performances of the two trigger functions: 1) a frontal/outflow boundary environment (grid point *A*), 2) mountainous terrain with daytime high-based convection (grid point *B*), and 3) a Great Plains environment (grid point *C*). These grid points were selected because they represent commonly occurring convective situations that trigger functions encounter and must quantitatively evaluate for the likelihood of deep convection. The performance of each trigger function is evaluated by first examining the specific thermodynamic environment (i.e., model-generated sounding) encountered by that trigger and then evaluating contributions of each component of the trigger. While the selection of the grid points likely will affect the results of the comparisons, this exercise nonetheless provides a framework for discussing the validity of the assumptions underlying the design of each trigger.

a. Frontal/outflow boundary environment

Figure 6 shows the model-generated 1200 UTC sounding for point *A*. This location is just ahead of the cold front and behind the deep clouds evident in Fig. 5. The boundary layer is stable (approximately isothermal) and relatively moist. Above the boundary layer the sounding is conditionally unstable, but parcels would have to overcome a substantial amount of convective inhibition. For example, even ignoring entrainment, parcels originating near the 850-mb level would have to be lifted nearly 200 mb before reaching their LFC. On the other hand, parcels originating from much higher levels, for example, near the 600-mb level, only require about 50 mb of lift to reach their LFC.

1) FC TRIGGER

Figure 7 shows the 1-h convective rainfall ending at 1300 UTC for the coarse-mesh simulation using the FC

TABLE 1. Component values for the FC trigger function for three different environments. Forecast time is time (UTC) at which convection is initiated, P_{SL} is the mean pressure of the source layer, P_{LCL} is the pressure of the lifting condensation level, T_{LCL} is the temperature of the rising parcel at its LCL, w_{res} is the resolvable-scale vertical velocity at the LCL, δT_{LCL} is the temperature perturbation applied to the parcel due to w_{res}, and T_{env} is the environmental temperature at the LCL.

	Grid point *A*	Grid point *B*	Grid point *C*
Forecast time (UTC)	1218	1236	1218
P_{SL} (mb)	600	670	813
P_{LCL} (mb)	589	560	719
T_{LCL} (°C)	−1.96	−6.01	8.17
w_{res} (m s^{-1})	.062	.046	.020
δT_{LCL} (°C)	1.85	1.68	1.27
T_{env} (°C)	−1.57	−4.49	9.26
Convection?	Yes	Yes	Yes

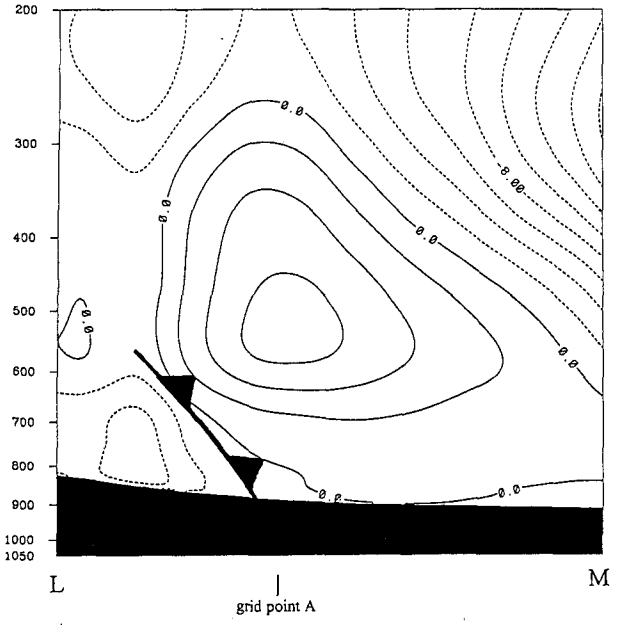

FIG. 8. Cross section of vertical motion through grid point *A* at 1200 UTC using the old trigger. Contour interval is 2 cm s^{-1}. Solid (dashed) lines denote upward (downward) motion.

trigger function. The trigger function initiated convection during the first hour in much of eastern Montana, including the location represented by point *A*. This is in contrast to the satellite imagery (Fig. 5), which indicates that the deep clouds were primarily over the northeast corner of Montana. Analysis of the components of the trigger function (Table 1) indicates that the mean level of the source layer for the convection is 600 mb and the LCL is 589 mb. The main factor that allows the convection to occur is the large boost that the trigger provides to the parcel as a result of pronounced midlevel upward motion associated with the frontal passage. Figure 8 shows a cross section of vertical motion through grid point *A* and the front. A core of maximum upward motion of 0.08 m s^{-1} is centered near 500 mb in the area immediately ahead of the front. The resolvable-scale vertical motion at the LCL is 0.062 m s^{-1}, giving a thermal perturbation of 1.85°C to the parcel (see Table 1). This is enough to give the parcel a higher temperature than the environment, so the FC trigger initiates deep convection.

With such a high source layer (300 mb above the surface), the decision to initiate convection in this case is questionable. Recall that the purpose of incorporating a forcing contribution from the resolvable-scale vertical velocity in the FC trigger function is to account for the organizing and strengthening effects of low-level convergence on hygrothermal/vertical velocity perturbations. However, since the source layer is so high in this case, the contribution by the midlevel vertical motion to organizing and strengthening low-level perturbations may be overestimated. Moreover, because this trigger function is so strongly linked with resolvable-scale vertical motion, and resolvable-scale vertical motion typically is maximized in the midtroposphere, there may be a tendency to prematurely (and erroneously) initiate convection from elevated source layers with high LCLs. As suggested in section 2, any linkage with resolvable-scale vertical motion should have some sort of dependence on height above the surface.

2) NEW TRIGGER

Unlike the FC trigger, the simulation using the new trigger function does not initiate convection in southeastern Montana during the first hour (not shown). Since the sounding representative of the local environment (Fig. 6) indicates that the boundary layer is stable over southeastern Montana, the only component contributing to the unmodified vertical velocity perturbation w_p is due to inhomogeneities. Table 2 lists the values of the various elements that contribute to the "decision" of the new trigger function at grid point A. The values have been computed for the same time and from the same source layer from which convection was initiated using the FC trigger. After accounting for the effects of convergence/divergence encountered by the parcel during ascent to its LFC, the magnitude of the final vertical velocity perturbation w' is 0.2 m s^{-1}. This is far less than the velocity perturbation needed to overcome the negative area between the source layer and the LFC (w_{neg} = 2.30 m s^{-1}), so convection does not occur. Another factor explaining the different "decisions" of the two triggers is the computation of convective inhibition (dark-shaded region in Fig. 6). Recall that in the FC scheme the convective inhibition between the source layer and the LCL is ignored.

TABLE 2. Same as in Table 1 except for the new trigger function. The expression w_i is the contribution to the total perturbation due to inhomogeneities, w_{cbl} is the contribution from a convective boundary layer if the source layer is within the boundary layer, w_{abl} is the contribution from a convective boundary layer if the source layer is above the boundary layer, $(\partial\omega/\partial p)_{SL}$ is the resolvable-scale convergence within the source layer, w' is the total perturbation, and w_{neg} is the inhibition between the source layer and the LFC.

	Grid point *A*	Grid point *B*	Grid point *C*
Forecast time (UTC)	1218	1236	1218
P_{SL} (mb)	600	670	813
P_{LCL} (mb)	589	560	719
w_i (m s^{-1})	0.22	0.21	0.49
w_{cbl} (m s^{-1})	0	0	0
w_{abl} (m s^{-1})	0	0	0
$(\partial\omega/\partial p)_{SL}$ (s^{-1})	0	2.3×10^{-4}	1.0×10^{-5}
w' (m s^{-1})	0.20	0.33	0.60
w_{neg} (m s^{-1})	2.30	10.80	6.01
Convection?	No	No	No

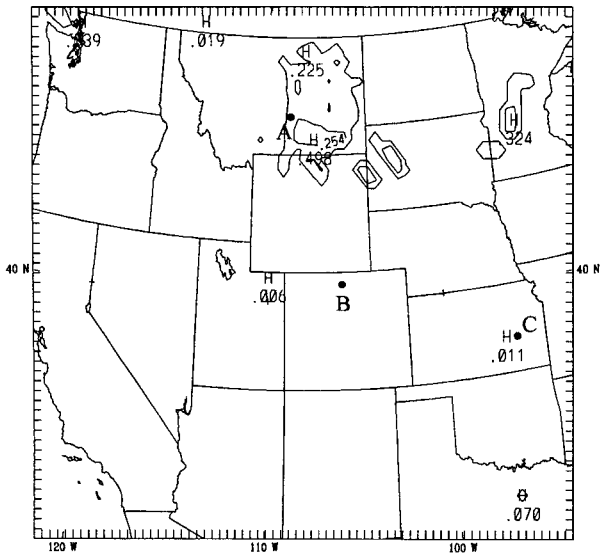

FIG. 9. One-hour accumulated convective rainfall for the coarse mesh ending at 1800 UTC using the new trigger function. First contour is 0.025 cm; second contour is 0.254 cm.

Therefore, a much smaller vertical velocity perturbation can trigger convection.

The new trigger continues to suppress convective activity at grid point *A* for 5 more hours. However, by 1800 UTC, convection is widespread over eastern Montana (Fig. 9). Figure 10 shows the 1700 UTC model sounding at point *A*, 10 min prior to the initiation of convection. The midtroposphere has dried, and a deep convective boundary layer (100 mb) has formed. A cross section passing through grid point *A* (not shown) reveals low-level upward motion over much of eastern Montana, including at point *A*. This upward motion, coupled with a growing convective boundary layer, has destabilized the environment to the point that convection can occur. Specifically, analysis of the trigger function at point A for the time convection is initiated (Table 3) indicates that the source layer for convection is just above the convective boundary layer. The decision to initiate convection depends upon vertical motion perturbations from two main sources: 1) inhomogeneities and 2) the underlying convective boundary layer. These sources of local vertical motion total 1.59 m s^{-1} and are sufficient to overcome the con-

TABLE 3. Same as in Table 2 except for 1710 UTC at point *A*, 1635 UTC at point *B*, and 1800 UTC at point *C*.

	Grid point *A*	Grid point *B*	Grid point *C*
Forecast time (UTC)	1710	1635	1800
P_{SL} (mb)	756	526	934
P_{LCL} (mb)	747	510	860
w_i (m s^{-1})	0.50	0.11	0.67
w_{cbl} (m s^{-1})	1.70	2.35	1.54
w_{abl} (m s^{-1})	1.09	1.67	0
$(\partial\omega/\partial p)_{SL}$ (s^{-1})	0	0	5.0×10^{-5}
w' (m s^{-1})	1.59	1.78	2.94
w_{neg} (m s^{-1})	1.56	1.56	9.30
Convection?	Yes	Yes	No

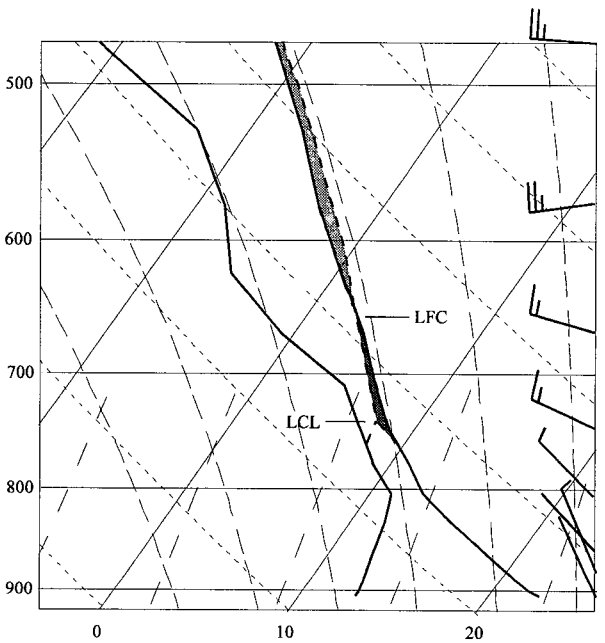

FIG. 10. Same as in Fig. 6 except for grid point *A* at 1700 UTC using the new trigger function.

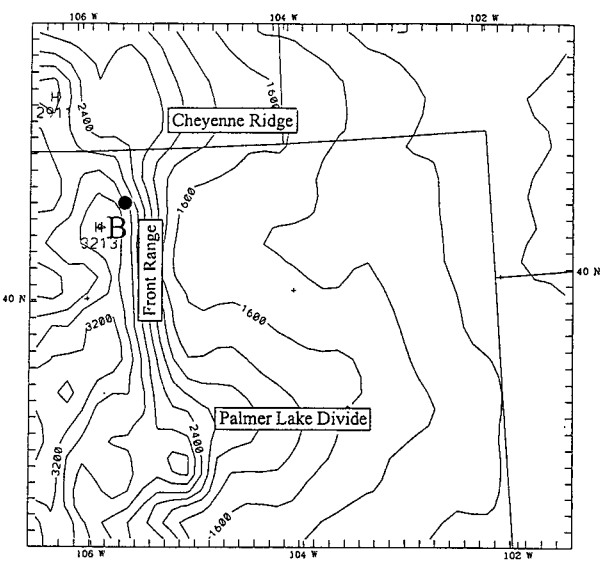

FIG. 11. Plot of fine-mesh terrain centered over northeast Colorado. Contour interval is 200 m.

vective inhibition of 1.56 m s^{-1}. Therefore, convection occurs, in contradiction with observations (Fig. 5).

b. *Mountainous terrain with daytime high-based convection*

Northeast Colorado is characterized by sharply contrasting relief where the High Plains end abruptly at the Front Range (Fig. 11). Oriented perpendicular to the Front Range are two east–west ridges, the Cheyenne Ridge and the Palmer Lake Divide. These east–west ridges and the Front Range are climatologically favorable regions for mountain-generated thunderstorms during the warm season (e.g., Henz 1974; Banta and Schaaf 1987). Storms generally form in the late morning after a convective boundary layer has developed and a mountain–valley circulation generates local confluence (Toth and Johnson 1985). Satellite images for this day indicate that the evolution of convection followed this conceptual model of development (Fig. 5).

1) FC TRIGGER

Figure 12 shows the 1-h convective rainfall ending at 1300 UTC for the fine-mesh simulation using the FC trigger function. It is evident that parameterized convection develops over many high-elevation locations (cf. Figs. 11 and 12). Figure 13 presents the 1200 UTC sounding for grid point *B*, 36 min before the initiation of convection. The location is along the high ridges of the Front Range (see Fig. 11). The boundary layer is dry and very stable, with a strong nocturnal inversion

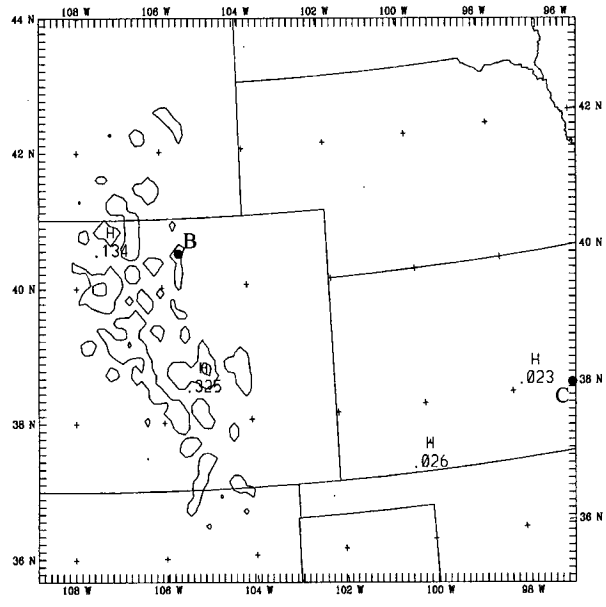

FIG. 12. One-hour accumulated convective rainfall for the fine mesh ending at 1300 UTC using the FC trigger function. First contour is 0.025 cm; second contour is 0.254 cm.

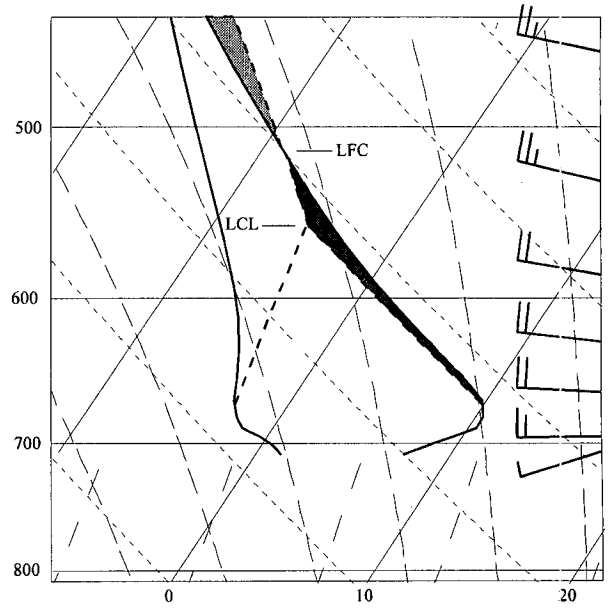

FIG. 13. Same as in Fig. 6 except for grid point *B* at 1200 UTC using the FC trigger function.

near the surface. Immediately above the inversion is a deep layer of nearly dry-adiabatic air. This dry-adiabatic layer is characteristic of a residual boundary layer created during the previous day's solar heating (Stull 1988). The presence of the inversion and the lack of moisture at the surface preclude convection from being initiated from the low levels. However, the possibility exists that convection may be initiated from layers between 700 and 600 mb.

Table 1 presents the values of the various elements composing the FC trigger function for a source layer centered at 670 mb. Recall that with the FC trigger the resolvable-scale vertical velocity at the LCL is used to modify the temperature of the parcel at the LCL before a comparison with the environmental temperature is made. In this case, the resolvable-scale vertical velocity is approximately 0.046 m s^{-1}, which the trigger converts to a positive thermal perturbation (analogous to a positive vertical velocity perturbation) of 1.68°C for the parcel. This is enough to cause the parcel temperature to be higher than the environmental temperature, so convection occurs.

Closer inspection of the sounding calls into question the decision to initiate convection here. In particular, the source-layer air must ascend 110 mb through very dry air before reaching saturation. In the FC trigger, the source-layer air is assumed to always reach its LCL and then, after addition of the thermal perturbation, is checked for buoyancy. However, because the source-layer air is 50 mb above the surface and above a strong inversion, thermal and/or vertical velocity perturbations would likely be weaker than if a well-mixed layer

were present. The assumption that the parcel will automatically reach its LCL neglects the inhibiting effect of the negative buoyancy and the entrainment of dry air encountered by the parcel during its 110-mb ascent to its LCL (dark-shaded region in Fig. 13). This inhibition likely would prevent the parcel from reaching its LCL. Therefore, convection should not have been triggered at this grid point.

2) NEW TRIGGER

In contrast to the FC trigger function formulation, the simulation with the new trigger function does not initiate widespread convection over the Front Range until the late morning, in agreement with the observations. Table 2 presents statistics from the trigger function for the same time and for the same source-layer air that were used with the FC trigger function. The only contribution to w_p comes from inhomogeneities ($w_i = 0.21$ m s^{-1}). This value of w_p is enhanced by the convergence that the parcel experiences during its ascent to its LFC. Nevertheless, the final value of the parcel perturbation w' is still less than w_{neg}, so convection does not occur here.

It is not until several hours into the simulation that convection is initiated at grid point *B*. The 1-h convective rainfall valid at 1700 UTC using the new trigger function is shown in Fig. 14. Scattered weak convection has occurred along the Front Range, including at grid point *B*. Figure 15 shows the 1600 UTC sounding at point *B*, 35 min before the initiation of convection.

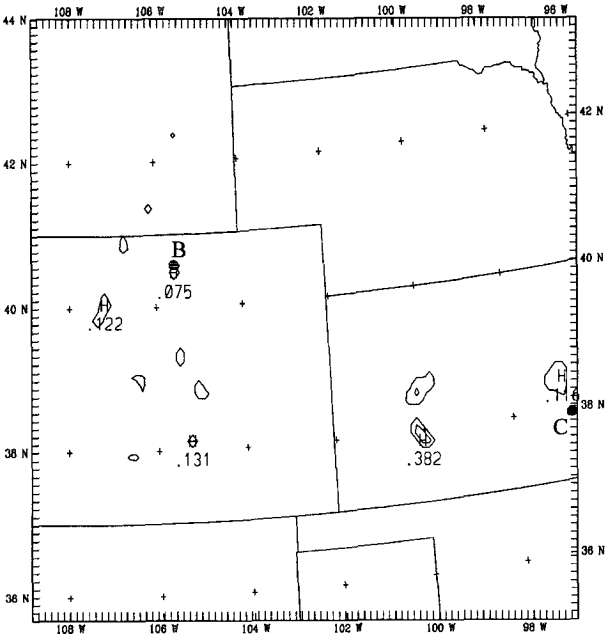

FIG. 14. One-hour accumulated convective rainfall for the fine mesh ending at 1700 UTC using the new trigger function. First contour is 0.025 cm; second contour is 0.254 cm.

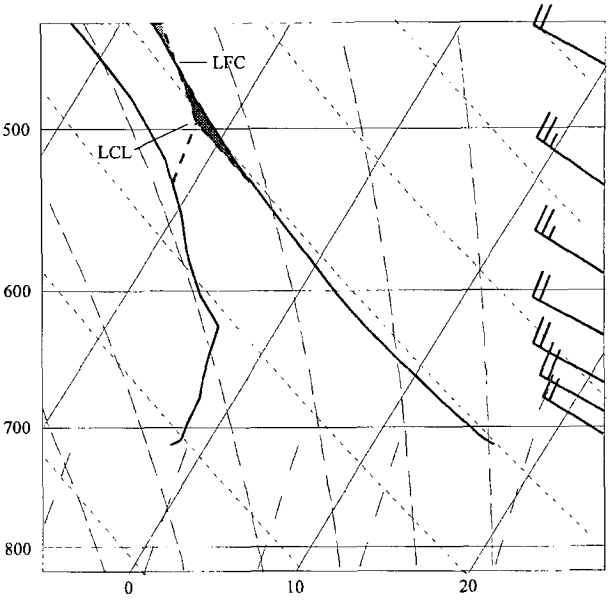

FIG. 15. Same as in Fig. 6 except for grid point *B* at 1600 UTC using the new trigger function.

A deep convective boundary layer (100 mb) has developed, but parcels emanating from this layer still must overcome a substantial amount of negative area in order to reach their LFC. However, grid point *B* is within a region of strong upward motion in the lower and middle troposphere (cross section not shown). This upward motion serves to destabilize the sounding during the next 35 min, especially in the middle troposphere. Statistics from the trigger function (Table 3) show that the source layer for the convection is above the convective boundary layer. Even after weakening the magnitude of the perturbation to account for this fact, the magnitude of the perturbation w' is 1.78 m s^{-1}. This is large enough to overcome the negative area between the source layer and the LFC ($w_{neg} = 1.56$ m s^{-1}), so convection occurs.

Comparisons with observations show that the evolution of convection over this area using the new trigger function follows more closely the observed patterns of convective development for the warm season on undisturbed days. Mountain-generated storms generally do not develop here until several hours after a morning convective boundary layer has formed (e.g., between 1000 and 1100 local time or 1600 and 1700 UTC). Using the new trigger, isolated pockets of convection did not develop until 1600 UTC. This contrasts sharply with the simulation using the FC trigger, where much of the Front Range and the Rockies of central Colorado were experiencing convection after the first hour. The sounding at the location where convection was initiated using the new trigger (Fig. 15) shows that the environment was similar to the typical environmental evolution preceding thunderstorm formation along the Front

Range (Toth and Johnson 1985), that is, the development of a convective boundary layer indicative of the development of a mountain–valley circulation.

c. *Great Plains environment*

The 1200 UTC model-generated sounding for grid point *C* in southeastern Kansas (Fig. 16) indicates a large amount of potential buoyant energy for the layer of air below 900 mb. However, due to the deep stable layer in the lowest 150 mb, the possibility of realizing this potential is remote. Satellite images during the first 7 h (Fig. 5) show that over much of Kansas convection does not occur. There are some low-level clouds over eastern Kansas throughout the time period, but deep convection is not evident anywhere in the region except over extreme eastern Kansas and central Missouri. No deep convection is observed over grid point *C* during this time period.

1) FC TRIGGER

Examination of the 1-h convective rainfall ending at 1300 UTC for the coarse-mesh simulation using the FC trigger function (Fig. 7) shows that this trigger initiated convection over most of eastern Kansas, including grid point *C*. Convection began at point *C* 18 min into the simulation. Referring to Table 1, there is an elevated source layer for the convection and about 100 mb of lift necessary for the source-layer air to reach its LCL. Nevertheless, as a result of the positive resolvable-scale vertical velocity at the LCL, the FC scheme provides a large thermal perturbation to the parcel, thereby enabling it to reach a higher temperature than its environment at the LCL. This is sufficient for the FC scheme to trigger convection. Inspection of convective rain plots for the next several hours (not shown) shows that this basic pattern of convection over Kansas persists. The source layers for the convection at grid point *C* during these hours remain in the 800–820-mb range.

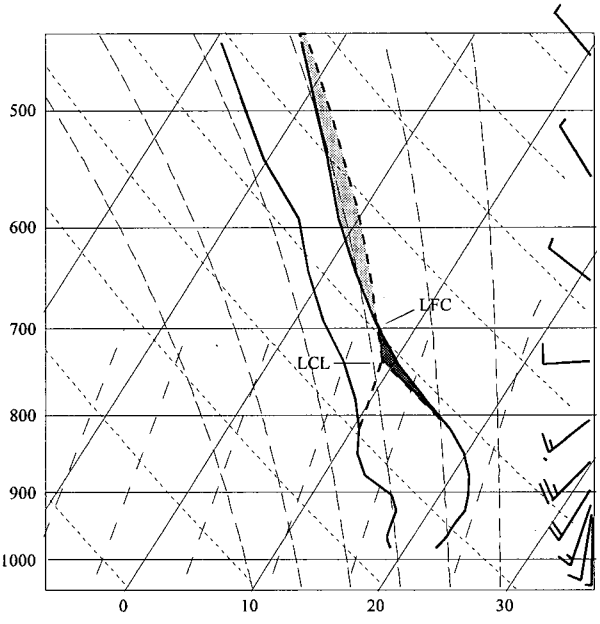

FIG. 16. Same as in Fig. 6 except for grid point *C* at 1200 UTC using the FC trigger function.

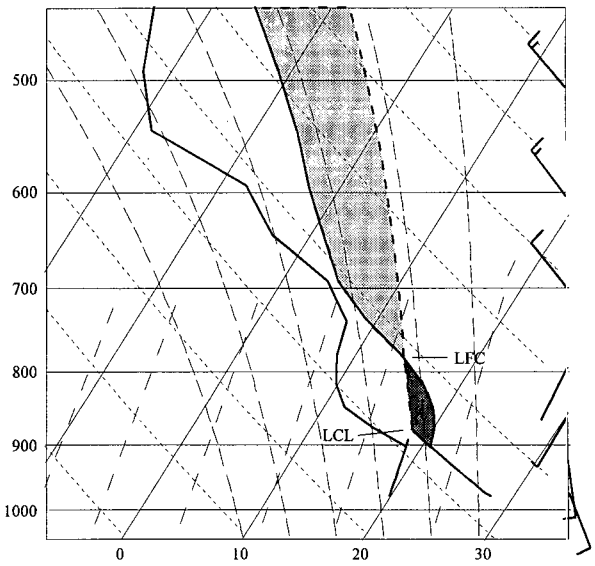

FIG. 17. Same as in Fig. 6 except for grid point *C* at 1800 UTC using the new trigger function.

The means by which convection is initiated by the FC trigger in this case are similar to how convection is initiated for the mountainous environment described previously. The source layer for the convection is within the nearly dry adiabatic layer aloft. This source-layer air must ascend almost 100 mb before reaching its LCL. Because the FC trigger assumes the parcel will reach its LCL, all of the inhibition that would be encountered during that ascent is neglected. The FC scheme does, however, correctly diagnose that the boundary layer air cannot overcome the deep stable layer just above the surface.

2) NEW TRIGGER

The simulation using the new trigger function produces a very different distribution of convection over the Plains than the simulation using the FC trigger. Specifically, during the entire 12 h of the simulation, most of Kansas remains free of convection. This is in stark contrast to the simulation using the FC trigger, where most of the state experiences convection during the first 6 h. The decision not to initiate convection using the new trigger can be understood by examining Table 2, which shows statistics from the new trigger for the same time and from the same source layer that the FC trigger initiated convection. Because the boundary

layer is stable, the only contribution to the vertical velocity perturbation comes from w_i. The parcel does encounter some convergence within the source layer, which strengthens the magnitude of the perturbation to 0.60 m s^{-1}. However, this is still considerably less than what is needed to overcome the amount of negative area encountered by the parcel (w_{neg} = 6.01 m s^{-1}). Therefore, convection does not occur.

The new trigger continues to inhibit deep convection even after a convective boundary layer has formed. Figure 17 shows the model-generated sounding for grid point *C* at 1800 UTC (1200 local time). A convective boundary layer extends 100 mb above the surface. Above the boundary layer is the remnant of the inversion present in the 1200 UTC sounding (Fig. 16). In spite of the development of the convective boundary layer, a significant amount of convective inhibition remains to be overcome. Table 3 shows that even with a contribution from the convective boundary layer (w_{cbl}) and resolvable-scale convergence, the final value for the perturbation w' is insufficient to overcome the convective inhibition, so convection does not occur.

5. Summary and concluding remarks

A general framework for defining convective trigger functions for mesoscale numerical models was presented. The basis for the framework is that the triggering decision rests with two fundamental steps:

1) estimation of the magnitude of the largest subgrid-scale vertical velocity perturbation originating from within each potential source layer, and
2) calculation of whether or not the perturbation is strong enough to overcome the grid-resolvable negative inhibition between the source layer and the LFC.

Within this framework, a new trigger function formulation that calculates the accessibility of potential buoyant energy by subgrid-scale perturbations was proposed. The formulation represents an improvement over previous schemes in the way in which it diagnoses accessibility to buoyant energy. It is expected that this improvement will give the trigger applicability to a wide variety of convective environments, ranging from well-mixed, free convective boundary layers to stably stratified, nocturnal boundary layers.

A test case exhibiting a variety of environments was selected for simulation using a mesoscale model. The effectiveness of the new trigger in diagnosing the onset of convection for three types of environments encountered by the model (a frontal/outflow boundary environment, mountainous terrain with daytime high-based convection, and a Great Plains environment) was assessed and compared with the performance of the FC trigger. In each of the three environments, the new trigger function performed better than the original FC formulation. In particular, the FC trigger prematurely initiated convection, while the new trigger slowed or eliminated convective development. The tendency of the FC trigger to initiate convection prematurely is attributable to two main factors. First, the FC trigger neglects the inhibition between the source layer and the LCL of the parcel, so that perturbations have a smaller amount of inhibition to overcome than if this negative area were included. Second, the FC trigger defines the magnitude of the perturbations based on the resolvable-scale vertical velocity at the LCL. Since vertical motion typically increases with height, the perturbation magnitudes increase as LCL heights increase. Convection is therefore more likely to be initiated earlier and from a higher source layer than what often seems physically reasonable.

The new trigger function addresses both of these issues. First, it accounts for the inhibition between the source layer and the LCL through its integration of the parcel buoyancy equation. Therefore, the total amount of inhibition that the rising parcel encounters is considered. Second, rather than *defining* a perturbation based on resolvable-scale upward motion, the new trigger takes an *existing* perturbation and *modifies* it based on the resolvable-scale convergence/divergence obtained by applying the continuity equation within the layer being considered. Because the magnitudes of the existing perturbations decrease with height, the impact of any increase with height of convergence/divergence is limited. Further, since convergence/divergence typically does not increase with height like vertical motion (Palmén and Newton 1969), the final perturbation magnitudes are not as sensitive to height.

While the new trigger function addresses the major components involved in assessing the likelihood of convection, there are several aspects that need refinement. First, a stronger link with resolvable-scale upward motion is needed. This is in recognition of the fact that organized convection relies upon a focused area of upward motion to destabilize the environment and focus the convection (e.g., mesoscale convective systems). These areas of upward motion are typically resolved by mesoscale models, and a functionality relating the likelihood of convection to this upward motion would increase the chances of reproducing these convective systems. Second, a more effective way of handling the transition to a late afternoon/evening boundary layer is needed. With the formulation presented here, once the boundary layer is no longer free convective, a major contributor to the total magnitude of the vertical velocity perturbation (often 60%–70%) is abruptly lost. This loss may prematurely end convection in the early evening hours. Third, allowing for mixing of the rising subsaturated parcel with the environment would more realistically diagnose the likelihood that the parcel could reach its LFC, especially in dry environments. Such entrainment would lower the θ_e of the parcel, reducing the depth of the cloud or inhibiting its formation altogether. Inclusion of this process likely would have prevented the spurious initiation of convection at grid point *A*. Fourth, a more

precise functionality with respect to surface properties (e.g., land-use categories, terrain profiles) would more accurately capture the generation of perturbations from inhomogeneities. Fifth, a contribution to account for free-atmospheric perturbations created by processes such as subgrid-scale gravity waves and Kelvin–Helmholtz waves would increase the possibility of convective initiation from elevated source layers in the absence of convective boundary layers. Finally, observational studies investigating all the proposed functionalities would allow for a more precise formulation to be developed.

We recognize, of course, that examination of the performance of a trigger at a few grid points for a single case is not a satisfactory measure of the robustness of its formulation. Furthermore, many of the formulations of this trigger lack a firm rooting in either an empirical or a theoretical framework, but only because no such framework exists in the literature. Nevertheless, important inferences were made about the validity of the physical assumptions underlying each trigger by examining their decisions given the boundary layer structure, perturbation sources, and resolvable-scale circulations. Moreover, the comparison of the performance of the two triggers during the first hour of the simulation is considered to be especially meaningful since the differences between the environments encountered by the two trigger functions were very small at this time.

While the results for this test case are encouraging, it is recognized that much further testing will be necessary to ascertain whether or not the new trigger will be able to function successfully in the spectrum of environments encountered by operational models.

Acknowledgments. The authors are grateful to several people who provided insight and valuable discussion regarding the physical principles and modeling considerations with respect to triggering convection. In particular, we wish to thank Drs. Jack Kain, Nelson Seaman, Dave Stauffer, and George Young for their help. Our gratitude is also extended to Diana Bartels and Dick Pritchard, who provided the satellite data, and to John Murphy, who provided the radar data. The research presented here was supported by the Department of the Army through Grant NDSEGF DAAL03-92-G-0331 and by the National Science Foundation through Grant ATM 92-22017.

REFERENCES

Arakawa, A., and W. H. Schubert, 1974: Interaction of a cumulus cloud ensemble with the large-scale environment, Part I. *J. Atmos. Sci.*, **31,** 674–701.

Avissar, R., and R. A. Pielke, 1989: A parameterization of heterogeneous land surfaces for atmospheric numerical models and its impact on regional meteorology. *Mon. Wea. Rev.*, **117,** 2113–2136.

Banta, R. M., and C. B. Schaaf, 1987: Thunderstorm genesis zones in the Colorado Rocky Mountains as determined by traceback of geosynchronous satellite images. *Mon. Wea. Rev.*, **115,** 463–476.

Chen, C., and H. D. Orville, 1980: Effects of mesoscale convergence on cloud convection. *J. Appl. Meteor.*, **19,** 256–274.

Chen, F., and R. Avissar, 1994: The impact of land-surface wetness heterogeneity on mesoscale heat fluxes. *J. Appl. Meteor.*, **33,** 1323–1340.

Clark, T. L., T. Hauf, and J. P. Kuettner, 1986: Convectively forced internal gravity waves: Results from two-dimensional numerical experiments. *Quart. J. Roy. Meteor. Soc.*, **112,** 899–925.

Dudhia, J., 1989: Numerical study of convection observed during the winter monsoon experiment using a mesoscale two-dimensional model. *J. Atmos. Sci.*, **46,** 3077–3107.

Emanuel, K. A., and D. J. Raymond, Eds., 1993: *The Representation of Cumulus Convection in Numerical Models. Meteor. Monogr.*, No. 46, Amer. Meteor. Soc., 246 pp.

Frank, W. M., and C. Cohen, 1985: Properties of tropical cloud ensembles estimated using a cloud model and an observed updraft population. *J. Atmos. Sci.*, **42,** 1911–1928.

Fritsch, J. M., and C. F. Chappell, 1980: Numerical prediction of convectively driven mesoscale pressure systems. Part I: Convective parameterization. *J. Atmos. Sci.*, **37,** 1722–1733.

Grell, G. A., J. Dudhia, and D. R. Stauffer, 1994: A description of the fifth-generation Penn State/NCAR Mesoscale Model (MM5). NCAR/TN-398 + STR, National Center for Atmospheric Research, Boulder, CO, 138 pp.

Henz, J. F., 1974: Colorado High Plains thunderstorm systems—A descriptive radar-synoptic climatology. M.S. thesis, Department of Atmospheric Sciences, Colorado State University, 82 pp.

Hong, X., M. J. Leach, and S. Raman, 1995: A sensitivity study of convective cloud formation by vegetation forcing with different atmospheric conditions. *J. Appl. Meteor.*, **34,** 2008–2028.

Kain, J. S., and J. M. Fritsch, 1990: A one-dimensional entraining/detraining plume model and its application in convective parameterization. *J. Atmos. Sci.*, **47,** 456–475.

——, and ——, 1992: The role of the convective "trigger function" in numerical forecasts of mesoscale convective systems. *Meteor. Atmos. Phys.*, **49,** 93–106.

——, and ——, 1993: Convective parameterization for mesoscale models: The Kain–Fritsch scheme. *The Representation of Cumulus Convection in Numerical Models, Meteor. Monogr.*, No. 46, Amer. Meteor. Soc., 165–170.

Khalsa, S. J. S., and G. K. Greenhut, 1985: Conditional sampling of updrafts and downdrafts in the marine atmospheric boundary layer. *J. Atmos. Sci.*, **42,** 2550–2562.

Kreitzberg, C. W., and D. J. Perkey, 1976: Release of potential instability. Part I: A sequential plume model within a hydrostatic primitive equation model. *J. Atmos. Sci.*, **33,** 456–475.

Kuo, H. L., 1974: Further studies of the parameterization of the influence cumulus convection on large scale flow. *J. Atmos. Sci.*, **31,** 1232–1240.

Palmén, E., and C. W. Newton, 1969: *Atmospheric Circulation Systems.* Academic Press, 603 pp.

Segal, M., W. E. Schreiber, G. Kallos, J. R. Garratt, A. Rodi, J. Weaver, and R. A. Pielke, 1989: The impact of crop areas in northeast Colorado on midsummer mesoscale thermal circulations. *Mon. Wea. Rev.*, **117,** 809–825.

Stensrud, D. J., 1992: Southward burst mesoscale convective systems: An observational and modeling study. Ph.D. thesis, The Pennsylvania State University, 184 pp.

——, and J. M. Fritsch, 1994: Mesoscale convective systems in weakly forced large-scale environments. Part III: Numerical simulations and implications for operational forecasting. *Mon. Wea. Rev.*, **122,** 2084–2104.

Stull, R. B., 1988: *An Introduction to Boundary Layer Meteorology.* Kluwer Academic, 666 pp.

Toth, J. J., and R. H. Johnson, 1985: Summer surface flow characteristics over northeast Colorado. *Mon. Wea. Rev.*, **113,** 1458–1469.

Zhang, D.-L., and R. A. Anthes, 1982: A high resolution model of the planetary boundary layer-sensitivity tests and comparisions with SESAME-79 data. *J. Appl. Meteor.*, **21,** 1594–1609.

——, H.-R. Chang, N. L. Seaman, T. T. Warner, and J. M. Fritsch, 1986: A two-way interactive nesting procedure with variable terrain resolution. *Mon. Wea. Rev.*, **114,** 1330–1339.